Measuring CP nature of top-Higgs couplings at the future Large Hadron electron Collider

Baradhwaj Coleppa [a], Mukesh Kumar [b,*], Satendra Kumar [a], Bruce Mellado [c]

[a] *Department of Physics, Indian Institute of Technology Gandhinagar, Gandhinagar 382 355, India*
[b] *National Institute for Theoretical Physics, School of Physics and Mandelstam Institute for Theoretical Physics, University of the Witwatersrand, Johannesburg, Wits 2050, South Africa*
[c] *University of the Witwatersrand, School of Physics, Private Bag 3, Wits 2050, South Africa*

A B S T R A C T

We investigate the sensitivity of top-Higgs coupling by considering the associated vertex as CP phase (ζ_t) dependent through the process $p\,e^- \to \bar{t}\,h\,\nu_e$ in the future Large Hadron electron Collider. In particular the decay modes are taken to be $h \to b\bar{b}$ and $\bar{t} \to$ leptonic mode. Several distinct ζ_t dependent features are demonstrated by considering observables like cross sections, top-quark polarisation, rapidity difference between h and $\bar{t}$ and different angular asymmetries. Luminosity (L) dependent exclusion limits are obtained for ζ_t by considering significance based on fiducial cross sections at different σ-levels. For electron and proton beam-energies of 60 GeV and 7 TeV respectively, at $L = 100$ fb^{-1}, the regions above $\pi/5 < \zeta_t \leq \pi$ are excluded at 2σ confidence level, which reflects better sensitivity expected at the Large Hadron Collider. With appropriate error fitting methodology we find that the accuracy of SM top-Higgs coupling could be measured to be $\kappa = 1.00 \pm 0.17(0.08)$ at $\sqrt{s} = 1.3(1.8)$ TeV for an ultimate $L = 1$ ab^{-1}.

© 2017 The Author(s). Published by Elsevier B.V. This is an open access article under the CC BY license (http://creativecommons.org/licenses/by/4.0/). Funded by SCOAP³.

1. Introduction

The recent discovery of the Higgs boson at the Large Hadron Collider (LHC) serves as the last step in establishing the particle content of the Standard Model (SM). The next step that has been undertaken is the characterisation of its properties regarding spin, CP-nature and the nature of interaction with other particles. While the spin-0 nature of the Higgs boson has been established by the experiments [1–5] and a complete CP-odd nature excluded at a 99.98% confidence limit (C.L.) [6,7], the possibility remains that the Higgs boson could still be an admixture of CP-odd and even states. Investigation of this possibility in a future Large Hadron electron Collider (LHeC) is the goal of this article via a detailed analysis of the associated production of the Higgs boson with an anti-top quark.

Since in the SM the Higgs boson coupling to fermions is directly proportional to the mass of the fermions, the Yukawa coupling associated with the third generation is important in the context of investigating the properties of the Higgs boson. Deviations in the top-Higgs coupling directly affect the production cross section of Higgs boson at the colliders, while changes in the bottom-Higgs coupling affect the total branching ratios.

Here we study the associated production of the Higgs boson with an anti-top quark at the future e^-p collider which employs a 7 TeV proton beam from a circular pp collider, and electrons from an Energy Recovery Linac (ERL) being developed for the LHeC [8,9]. The choice of an ERL energy of electron of $E_e = 60$ to 120 GeV, with available proton beam energy $E_p = 7$ TeV provides centre of mass energy of $\sqrt{s} \approx 1.3$ to 1.8 TeV. While the LHC is clearly energetically superior, the LHeC configuration is advantageous for the following reasons: (i) since initial states are asymmetric, backward and forward scattering can be disentangled, (ii) it provides a clean environment with suppressed backgrounds from strong interaction processes and free from issues like pile-ups, multiple interactions etc. (iii) such machines are known for high precision measurements of the dynamical properties of the proton allowing simultaneous tests of electroweak and QCD effects. A detailed report on the physics and detector design concepts of the LHeC can be found in the Ref. [8]. A distinguishing feature of the e^-p collider is that the production of the Higgs is only due to electroweak processes [10,11] and as noted above, since the e^- and p energies are different, the machine can also produce interesting patterns of

* Corresponding author.
E-mail addresses: baradhwaj@iitgn.ac.in (B. Coleppa), mukesh.kumar@cern.ch (M. Kumar), satendrak@iitgn.ac.in (S. Kumar), bruce.mellado@wits.ac.za (B. Mellado).

kinematic distributions that one can exploit to explore the CP nature of the Higgs boson.

Denoting the CP-odd (CP-even) components of the top-Higgs coupling by C_t^P (C_t^S), the updated bound on the CP top-Higgs couplings by combining the LHC Run-1 and Run-2 Higgs data sets allows the ranges $|C_t^P| < 0.37$ and $0.85 < C_t^S < 1.20$, which is stronger than the previous LHC Run-1 bound $|C_t^S| < 0.54$ and $0.68 < C_t^S < 1.20$. We note here that a future precision measurement of the process $e^+ e^- \rightarrow h\gamma$ with an accuracy of 0.5% will be able to constrain $|C_t^P| < 0.19$ at a 240 GeV $e^+ e^-$ Higgs factory [12]. Various studies on anomalous top-Higgs coupling in associated production of Higgs and top quark can be found in [13–16].

The article is organised as follows: We discuss the formalism by introducing a generalised CP-phase dependent top-Higgs coupling Lagrangian in Section 2. In Section 3 simulation and parton-level analyses of the process emphasising relevant kinematic observables are discussed. Also in this section we provide luminosity dependent exclusion limits of phases corresponding to the top-Higgs coupling. Finally, in Section 4 we conclude with inferences and summary. Though the whole focus of this study is in the LHeC environment, we also discuss and compare our results with those expected at the LHC.

2. Formalism

In the SM, the Yukawa coupling of the third generation of quarks is given by

$$\mathcal{L}_{\text{Yukawa}} = -\frac{m_t}{v} \bar{t} t h - \frac{m_b}{v} \bar{b} b h, \tag{1}$$

where $v \equiv \left(\sqrt{2} G_F\right)^{-1/2} = 2 m_W / g \simeq 246$ GeV, and m_t (m_b) is the mass of the top (bottom) quark. Due to the pure scalar nature of the Higgs boson in the SM, here the top- and bottom-Higgs couplings are completely CP-even. To investigate any beyond the SM (BSM) nature of the Higgs-boson as a mixture of CP-even and CP-odd states, we write a CP-phase dependent generalised Lagrangian as follows [17]:

$$\mathcal{L} = -\frac{m_t}{v} \bar{t} \left[\kappa \cos \zeta_t + i \gamma_5 \sin \zeta_t\right] t \, h$$
$$- \frac{m_b}{v} \bar{b} \left[\cos \zeta_b + i \gamma_5 \sin \zeta_b\right] b \, h. \tag{2}$$

Here ζ_t and ζ_b are the phases of the top-Higgs and bottom-Higgs couplings respectively. It is clear from the Lagrangian in Eq. (2) that $\zeta_{t,b} = 0$ or $\zeta_{t,b} = \pi$ correspond to a pure scalar state while $\zeta_{t,b} = \frac{\pi}{2}$ to a pure pseudo scalar state. Thus, the ranges $0 < \zeta_{t,b} < \pi/2$ or $\pi/2 < \zeta_{t,b} < \pi$ represent a mixture of the different CP-states. The case $\kappa = 1$, $\zeta_t = 0$ corresponds to the SM. In terms of C_t^S and C_t^P, we can also translate $\zeta_t = \tan^{-1}(C_t^P / C_t^S)$.

At the LHeC, the top-Higgs couplings can be probed via associated production of Higgs-boson with anti-top quark $p e^- \rightarrow \bar{t} h \nu_e$ – it is thus necessary to consider a 5-flavour proton including the b-quark parton distribution. The Feynman diagrams for the process under investigation are shown in Fig. 1. It is important to notice that in this process three important couplings are involved, namely hWW, Wtb and the top-Higgs (tth). A detailed study of hWW and Wtb couplings at the $e^- p$ collider have been performed in Refs. [11,18] and [19], respectively. For our studies we do not consider the BSM bottom-Higgs coupling since the effect of the phase ζ_b on the total production cross section or kinematics of top-Higgs production at the LHeC are negligible. Thus in what follows, we simply set $\zeta_b = 0$.

As noted in Ref. [17] in the context of the LHC, quantitatively an interesting feature can be observed: in the pure SM case there
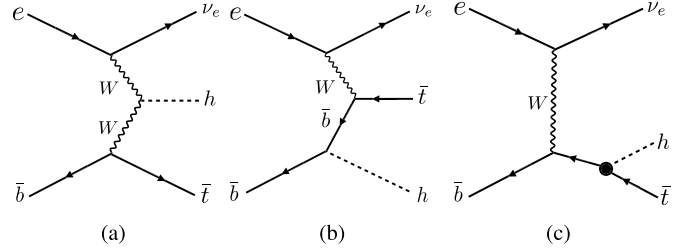

Fig. 1. Leading order Feynman diagrams contributing to the process $p e^- \rightarrow \bar{t} h \nu_e$ at the LHeC. The black dot in the Feynman diagram (c) denotes the top-Higgs coupling which is the subject of this study.
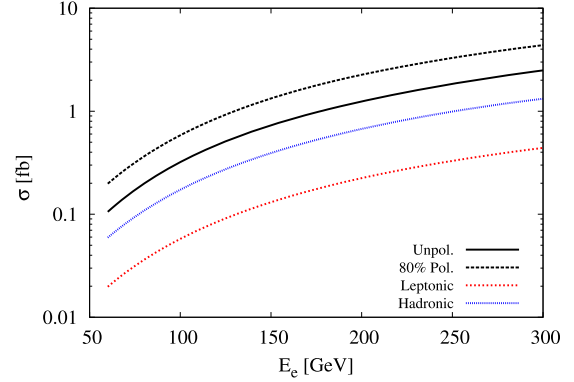

Fig. 2. Total cross section of the associated top-Higgs production against electron beam energy for fixed $E_p = 7$ TeV. The dotted and solid *black* lines correspond to the process $p \, e^- \rightarrow \bar{t} \, h \, \nu_e$ with and without polarisation of electron beam respectively. The dotted *red* and *blue* lines correspond to $\sigma \times$ BR for the leptonic and hadronic decay modes of $\bar{t}$ where for this estimation we use basic cuts as given in text. (For interpretation of the references to colour in this figure legend, the reader is referred to the web version of this article.)

is constructive interference between the diagrams shown in Fig. 1a and Fig. 1c for $\zeta_t > \pi/2$ resulting in an enhancement in the total production cross section of associated top-Higgs significantly. This is also true for $\zeta_t < \pi/2$ – however the degree of enhancement is much smaller owing to the flipped sign of the CP-even part of the coupling.

3. Simulation and analysis

We begin our study to probe the sensitivity of the top-Higgs couplings in terms of ζ_t by building a model file for the Lagrangian in Eq. (2) using FeynRules [20], and then simulating the charged current associated top-Higgs production channel $p e^- \rightarrow \bar{t} h \nu_e$ (see Fig. 1), with h further decaying into a $b\bar{b}$ pair and the $\bar{t}$ decaying leptonically in the LHeC set-up with centre of mass energy of $\sqrt{s} \approx$ 1.3 TeV. In this article we perform the analysis at parton level only where for signal and background event generation we use the Monte Carlo event generator package MadGraph5 [21]. We use NN23LO1 [22,23] parton distribution functions for all event generations. The factorisation and renormalisation scales for the signal simulation are fixed at $\mu_F = \mu_R = (m_t + m_h)/4$ while background simulations are done with the default MadGraph5 [21] dynamic scales. The e^- polarisation is assumed to be – 80%. We now list and explain various kinematic observables that can serve as possible discriminants of a CP-odd $t\bar{t}h$ coupling.

3.1. Cross section studies

In Fig. 2, we present the variation of the total cross section against the electron beam energy for the signal process

Table 1

Cross sections of signal and backgrounds in charged current (cc), neutral current (nc) and photo-production (photo) modes for $E_e = 60$ GeV and $E_p = 7$ TeV as explained in the text. Here X could be either of missing energy or electron and j is all possible combinations of light-, c- and b-quarks and gluons. For this estimation we use basic cuts as mentioned in text and electron polarisation is taken to be – 0.8.

| Process	cc (fb)	nc (fb)	photo (fb)
Signal:	1.98×10^{-2}	–	–
$Wjjj + X$, \h	$2.05 \times 10^{+2}$	$3.18 \times 10^{+1}$	$3.40 \times 10^{+3}$
$Wjjj + X$, \t	$4.18 \times 10^{+1}$	$3.16 \times 10^{+1}$	$3.41 \times 10^{+3}$
$Wjjj + X$, \th	$4.16 \times 10^{+1}$	$3.18 \times 10^{+1}$	$3.41 \times 10^{+3}$
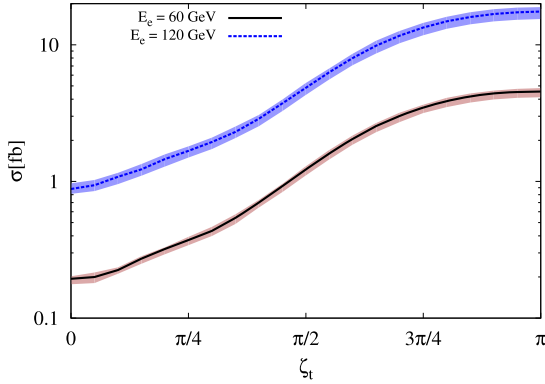
Fig. 3. Total cross section as a function of ζ_t with scale uncertainties. The *black* solid and *blue* dotted lines correspond to $E_e = 60$ and 120 GeV respectively for fixed $E_p = 7$ TeV and $\mu_F = \mu_R = (m_t + m_h)/4$. (For interpretation of the references to colour in this figure legend, the reader is referred to the web version of this article.)

$p\,e^- \rightarrow \bar{t} h \nu_e$, by considering un-polarised and – 80% polarised e^- beam. Also, the effect of branchings of $h \rightarrow b\bar{b}$ and the $\bar{t}$ decay for both leptonic and hadronic modes are shown. Possible background events typically arise from $W+$ multi-jet events, $Wb\bar{b}$ with missing energy which comes by considering only top-line (\h), only Higgs-line (\t) and without top- and Higgs-line (\th) in charged and neutral current deep-inelastic scattering and in photo-production by further decaying W into leptonic mode. In Table 1 we give an estimation of cross sections for signal and all possible backgrounds imposing only basic cuts on rapidity $|\eta| \leq 10$ for light-jets, leptons and b-tagged jets, the transverse momentum cut $p_T \geq 10$ GeV and $\Delta R_{\min}$[1] = 0.4 for all particles.

We now estimate the sensitivity of the associated top-Higgs production cross-section, $\sigma(\zeta_t)$, as a function of the CP phase of the tth-coupling as shown in Fig. 3 by considering $E_e = 60$ and 120 GeV with fixed $E_p = 7$ TeV. The scale uncertainties are taken as $(m_t + m_h)/8 \leq \mu_F = \mu_R \leq (m_t + m_h)/2$. Here $\sigma(\zeta_t = 0)$ corresponds to the SM cross section. We notice that the cross section is very sensitive to ζ_t in the region $\zeta_t > \frac{\pi}{2}$ where the interference between the diagrams becomes constructive. Below $\zeta_t = \frac{\pi}{2}$ the interference is still constructive though its degree decreases with ζ_t, thus increasing the cross section by around 500% at $\zeta_t = \frac{\pi}{2}$ which corresponds to the pure CP-odd case. On the other hand, for pure CP-even case $\zeta_t = \pi$ with opposite-sign of tth-coupling the cross section can be enhanced by up to 2400% for $E_e = 60$ GeV. Notice that for the case $E_e = 120$ GeV, $\sigma(\zeta_t)$ displays a similar shape with enhanced cross sections with respect to $E_e = 60$ GeV case. The scale uncertainty on an average is approximately 7(9)% for $E_e = 60(120)$ GeV in the whole range of ζ_t.
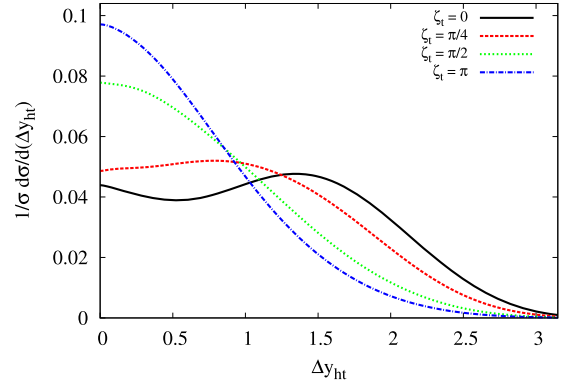
Fig. 4. The normalised difference between rapidities of top quark and the Higgs boson at some typical values of ζ_t for $E_e = 60$ GeV and $E_p = 7$ TeV. The *black* solid line corresponds to the SM case, while dotted lines correspond to different values of ζ_t. (For interpretation of the references to colour in this figure legend, the reader is referred to the web version of this article.)

However, it is quite interesting that the combined ATLAS and CMS measurements at $\sqrt{s} = 7$ and 8 TeV allow deviation of cross section in terms of signal strength $\mu = 2.3^{+0.7}_{-0.6}$ [24] for associated top-Higgs production.[2] Though one may investigate the possibilities of such observations due to comparatively heavy scalar with respect to the Higgs-boson as in Refs. [25,26].

3.2. Rapidity difference between the anti-top and the Higgs

In Refs. [11,18] it was suggested that in order to explore the tensorial spin-CP nature of hW^+W^- and hhW^+W^- vertices, azimuthal angle correlation between missing energy and scattered jets is a good observable. Also further studying the asymmetry based on such observables proves to be an excellent tool for any BSM nature of the associated couplings. Here and in the next subsections we include such observables in our studies with different combinations of final state particles as a function of ζ_t. We begin with the sensitivity of BSM aspects of the tth coupling in the rapidity difference between the anti-top quark and the Higgs boson distribution, Δy_{ht}.

In Fig. 4 we present the normalised Δy_{ht} distribution for a few chosen values of ζ_t. Any BSM physics effect can be observed by comparing the shape corresponding to the SM case $\zeta_t = 0$. We find that the distribution features for the different values of CP phase split into two distinguishable regions when $\Delta y_{ht} < 1$ and $1 < \Delta y_{ht} < 3$. In the former, most values of ζ_t are seen to correspond to distributions larger than the SM case, while the second region presents a complementary behaviour. The distortion in the shape for $\zeta_t > 0$ is the effect of mixing between CP-even and odd components of the tth vertex following the Lagrangian in Eq. (2). Overall, with the inclusion of spin-0^+ BSM admixture, the Δy_{ht} distribution is pushed towards lower values and acts as a potential discriminator to explore the CP-nature of tth-coupling. Similar studies are used to probe the tensor structure of hVV ($V = W^\pm, Z$) coupling at the LHC and one such study of the Higgs boson production in the vector boson fusion mode is performed in [27] by taking the rapidity difference between the Higgs and the leading parton.

---

[1] The distance parameter between any two particles is defined as $\Delta R = \sqrt{(\Delta\phi)^2 + (\Delta\eta)^2}$, where ϕ and η are the azimuthal angle and rapidity respectively of particles into consideration.

[2] Note that at the LHC the production of associated Higgs boson with top-quark is possible via double and single-top quarks and is different from LHeC where the environment and centre of mass energies are different. The signal strength is defined as $\mu = \sigma_{\text{observed}}/\sigma_{\text{SM}}$.
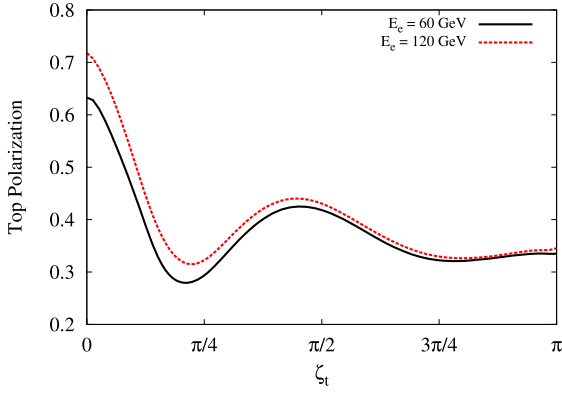
Fig. 5. The degree of longitudinal polarisation (P_t) of the top quark against ζ_t. The *black* solid and *red* dotted lines correspond to the $E_e = 60$ and 120 GeV, while E_p is fixed at 7 TeV. (For interpretation of the references to colour in this figure legend, the reader is referred to the web version of this article.)

3.3. Top quark polarisation

The large top-quark mass $m_t = 172.84 \pm 0.70$ GeV [28] indicates that the top could potentially play a singular role in the understanding of electroweak symmetry breaking in BSM scenarios. Since the decay width of the top exceeds $\Lambda_{\rm QCD}$, the top decays before hadronising and thus its spin information is preserved in the differential distribution of its decay products. With the Higgs coupling to top modified, it is reasonable to expect an asymmetry in the production of tops of different polarisations and the effect of ζ_t on this asymmetry.

We define the degree of longitudinal polarisation P_t of the top quark as

$$P_t = \frac{N_+ - N_-}{N_+ + N_-} \equiv \frac{\sigma_+ - \sigma_-}{\sigma_+ + \sigma_-}, \qquad (3)$$

where N_+ and N_- denote the number of events with positive and negative helicity anti-top quarks respectively, which can be rewritten in terms of the corresponding cross sections $\sigma_\pm$. In Fig. 5, we present P_t in the process $p\,e^- \to \bar{t}\,h\,\nu_e$ at the LHeC as a function of ζ_t. We obtain $N_\pm$ or $\sigma_\pm$ using the helicity amplitudes in MadGraph5. It can be seen from the plot that the degree of polarisation is quite sensitive over the entire range of ζ_t since the CP-odd coupling violates parity for any non-zero ζ_t. It is interesting to note that if Fig. 1c is the only diagram that contributed to P_t then the fraction of right-handedly polarized anti-top quark would increase as ζ_t increases from 0 and reach a maximum at $\zeta_t = \pi/2$ and then fall. However, the presence of other diagrams means that the plot is not symmetric about $\zeta_t = \pi/2$. The general features of P_t in Fig. 5 can be understood as the effect of interference among the diagrams in Fig. 1a, Fig. 1b (from where right-handed anti-top quarks are produced) and the Higgs-bremsstrahlung diagram Fig. 1c, which contains the CP-violating $\sin\zeta_t$ term.

As mentioned before, information of the spin of the top is preserved in its decay products and the angular distribution of its decay products can be parametrised as:

$$\frac{1}{\Gamma_f}\frac{d\Gamma_f}{d\cos\theta_f} = \frac{1}{2}(1 + \alpha_f P_t \cos\theta_f), \qquad (4)$$

where f is the type of top decay product, θ_f is the angle between f and the top-quark spin quantisation axis measured in the rest frame of the top-quark and Γ_f denotes the partial decay width corresponding to f. For the decay mode $t \to b + W^\pm (\to l^\pm + \nu_l)$ at lowest order, $\alpha_W = -\alpha_b = 0.39$, $\alpha_\nu = -0.3$, $\alpha_l = 1$ [29], with small QCD corrections to these values [30,31]. The charged lepton $l^\pm$ (or the down-type quark d in a hadronic decay of the intermediate W)

is nearly 100% correlated with the top quark spin which means that the $l^\pm$ or d is much more likely to be emitted in the direction of the top quark spin than in the opposite direction. It is a well known fact that the energy and momentum of leptons can be measured with high precision at the LHC and the same is true for the LHeC as well, so we focus on the leptonic decay mode of the anti-top for asymmetries in angular observable studies in what follows.

3.4. Cut-based event optimisation

Before discussing the angular observables for this study, it is important to discuss the optimisation of SM signal and background events as mentioned in Section 3.1. Angular observables are affected due to kinematic cuts and hence it is better to analyse events after optimising the signal with respect to backgrounds. The full SM signal process for this analysis is $p\,e^- \to \bar{t}\,h\,\nu_e$, with $h \to b\bar{b}$ and $\bar{t} \to W^-\bar{b}$, $W^- \to l^-\nu_l$ ($l^\pm = e^\pm, \mu^\pm$). After preliminary analysis of various kinematic distributions of final state particles of the SM signal and all possible leptonic backgrounds, we employ the following criteria to select events: (i) $p_T \geq 20$ GeV for b-tagged jets and light-jets, and $p_T \geq 10$ GeV for leptons. (ii) Since the LHeC collider is asymmetric, event statistics of final state particles are mostly accumulated on the left or right sides of the transverse plane $\eta = 0$ (depending on the initial direction of p and e^-) – we select events within $-2 \leq \eta \leq 5$ for b-tagged jets while $2 \leq \eta \leq 5$ for leptons and light-jets. (iii) The separation distance of all final state particles are taken to be $\Delta R > 0.4$. (iv) Missing transverse energy $\not{E}_T > 10$ GeV to select the top events. (v) Invariant mass windows for the Higgs through b-tagged jets and the top are required to be $115 < m_{bb} < 130$ GeV and $160 < m_t < 177$ GeV respectively, which are important to reduce the background events substantially. In these selections the b-tagging efficiency is assumed to be 70%, with fake rates from c-initiated jets and light jets to the b-jets to be 10% and 1% respectively. These constitute our event selection criteria which we use in the subsequent analysis.

There are two major difficulties in reconstructing the Higgs boson and the top in the process $p\,e^- \to \bar{t}\,h\,\nu_e \to (W^-\bar{b})h\nu_e \to l^-\nu_l b\bar{b}b\nu_e$: (a) Choosing appropriate b-tagged jets – in the final state we have 3 b-tagged jets with two originating from h decay and one from the decay of $\bar{t}$ and (b) the source of missing energy comes from both the production process and from $W^\pm$ decay. Since we performed parton-level analysis, we read the event files generated from the Monte Carlo generator and by reading appropriate identities we obtained information about the origin of b-tagged jets and neutrino and the corresponding four-momenta information was used for the analysis. Although the detector-level analysis is beyond the scope of this article, we mention briefly that for distinguishability of b-jets the solution is to take into account the p_T ordering of all b-tagged jets and since top-quark is heavier than the Higgs boson, the leading-p_T b-jet can identified as the decay product of top-quark, and the sub-leading and next to sub-leading p_T-ordered b-jets can be used to reconstruct Higgs boson.

To reconstruct the top, substantial requirement on missing energy and top-quark invariant mass formula $m_t^2 = (m_T + m_{b_1})^2$ can be used, where m_T is transverse mass observable to reconstruct W-boson and m_{b_1} is the mass of leading-b jet and is given as:

$$m_T = \sqrt{2\,p_T^l\,p_T^\nu\,(1 - \cos(\phi_l - \phi_\nu))},$$

where $\cos(\phi_l - \phi_\nu)$ is the angle between the electron and neutrino in the transverse plane, and ϕ_l (ϕ_ν) is the azimuthal angle of the electron (neutrino). However, it is to be noted that m_T is also inefficient when there are more than one source of missing energy and hence alternative method should be explored.
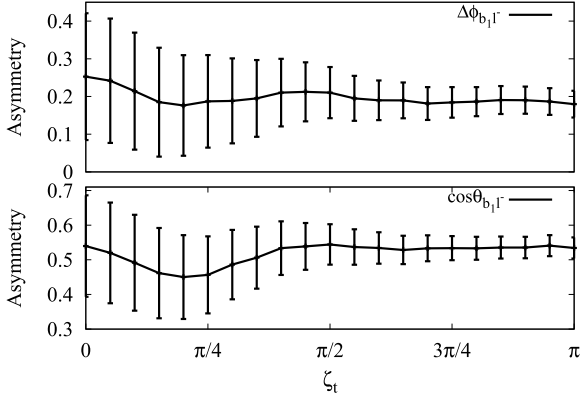
Fig. 6. Variation of angular asymmetries between the leading b-tagged jet and the charged lepton in the differential azimuthal and polar angle ($\Delta\phi_{b_1l^-}$ and $\cos\theta_{b_1l^-}$) distributions with respect to ζ_t for $E_e = 60$ GeV and $E_p = 7$ TeV. The error bars correspond to the uncertainties in asymmetry measurement at $L = 1\,\mathrm{ab}^{-1}$.

3.5. Angular observables in terms of asymmetries

After this short discussion on event selection criteria, we now discuss observables based on angular asymmetry between different final state particles. We construct the asymmetry from the differential distribution of kinematic observables using the final leptons and b-tagged jets. These asymmetries are studied only for signal processes as a function of ζ_t. The angular asymmetries with respect to polar angle[3] $\cos\theta_{ij}$ and the azimuthal angle difference $\Delta\phi_{ij}$ are defined to be:

$$A_{\theta_{ij}} = \frac{N_+^A(\cos\theta_{ij} > 0) - N_-^A(\cos\theta_{ij} < 0)}{N_+^A(\cos\theta_{ij} > 0) + N_-^A(\cos\theta_{ij} < 0)}, \quad (5)$$

$$A_{\Delta\phi_{ij}} = \frac{N_+^A(\Delta\phi_{ij} > \pi/2) - N_-^A(\Delta\phi_{ij} < \pi/2)}{N_+^A(\Delta\phi_{ij} > \pi/2) + N_-^A(\Delta\phi_{ij} < \pi/2)}, \quad (6)$$

where i and j are any two different final state particles. Using binomial distribution we use the following formula to calculate the statistical uncertainty (δ_α) in the measurement of these asymmetries (A_α):

$$\delta_\alpha = \sqrt{\frac{1 - A_\alpha^2(\zeta_t)}{\sigma_{\zeta_t} \cdot L}}, \qquad (\alpha = \theta_{ij}, \Delta\phi_{ij}) \quad (7)$$

where σ_{ζ_t} is the total cross section of signal events as a function of ζ_t and L is the total integrated luminosity.

In Fig. 6, we show the asymmetries between the charged lepton and the $\bar{b}$ from $\bar{t}$ decay (denoted by b_1 in the plot) as functions of ζ_t. We can see that the asymmetries in $\Delta\phi_{b_1\ell^-}$ and $\cos\theta_{b_1\ell^-}$ follow the top polarisation curve to some extent in that they fall till $\zeta_t \approx \pi/4$. We find that beyond $\zeta_t = \pi/2$, the curves flatten. As explained in the Section 3.3 the shapes in these asymmetry observables are also influenced by interference among the Feynman diagrams shown in Fig. 1. Overall we can conclude that these asymmetry observables can serve as good discriminators for a nonzero ζ_t, particularly for $\zeta_t < \pi/2$ where the difference from the $\zeta_t = 0$ case is more pronounced.

3.6. Exclusion limits

In Section 3.5 we observed that asymmetry observables based on differential distributions of $\cos\theta_{b_1l^-}$ and $\Delta\phi_{b_1l^-}$ show distinct
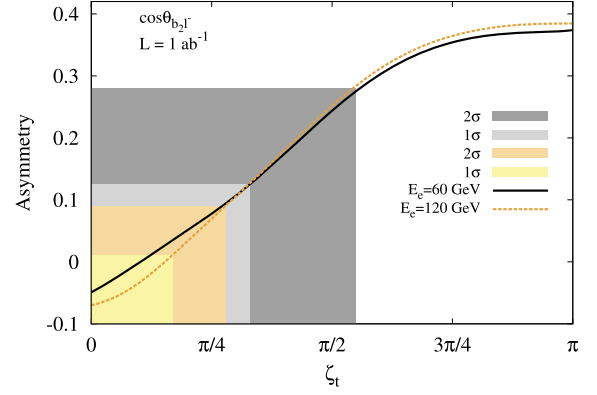
Fig. 7. Variation of the angular asymmetry between the subleading b-tagged jets and charged leptons in the differential polar angle ($\cos\theta_{b_2l^-}$) distribution with respect to ζ_t for $E_e = 60$ GeV (*black solid line*) and $E_e = 120$ GeV (*orange dashed line*) with $E_p = 7$ TeV. The shaded regions *grey* (*orange*) and *light grey* (*yellow*) correspond to 2σ and 1σ of statistical uncertainty in the measurement of the asymmetry in the SM for $E_e = 60\,(120)$ GeV at $L = 1\,\mathrm{ab}^{-1}$ respectively. (For interpretation of the references to colour in this figure legend, the reader is referred to the web version of this article.)

features in terms of shape although quantitatively not very sensitive. Therefore we construct another asymmetry observable by considering the polar angle between the sub-leading b-tagged jet and the lepton from W^- decay, i.e., $\cos\theta_{b_2l^-}$ which is comparatively more sensitive (quantitatively). In Fig. 7, we show the asymmetry $A_{\cos\theta_{b_2l^-}}$ as a function of ζ_t for $E_e = 60$ and 120 GeV with $E_p = 7$ TeV. The statistical uncertainties are calculated using the formula in Eq. (7) for $\zeta_t = 0$ and explicitly given as:

$$\delta A_{\cos\theta_{b_2l^-}} = \sqrt{\frac{1 - (A_{\cos\theta_{b_2l^-}}^{\mathrm{SM}})^2}{\sigma_{\mathrm{SM}} \cdot L}}, \quad (8)$$

where σ_{SM} is total cross section of the SM signal and $A_{\cos\theta_{b_2l^-}}^{\mathrm{SM}}$ is numerical value of corresponding SM asymmetry. Therefore at the luminosity of $L = 1\,\mathrm{ab}^{-1}$, $A_{\cos\theta_{b_2l^-}}$ used to determine ζ_t within $\pi/3$ and $3\pi/5$ ($\pi/6$ and $3\pi/10$) at 1σ and 2σ C.L. respectively for $E_e = 60\,(120)$ GeV. This indicates that at low L the sensitivity tends to be poorer than this, so next we use fiducial inclusive cross sections as another observable to find the exclusion limits.

Based on selection criteria of signal and background events discussed in Section 3.4, we estimated the exclusion regions of ζ_t as a function of L in fb^{-1}. The exclusion is based on significance using the Poisson formula $\mathcal{S} = \sqrt{2[(S+B)\log(1+S/B) - S]}$, where S and B are the number of expected signal and background events at a particular luminosity respectively. Here we used 10% systematic uncertainty for background yields only. In Fig. 8, we present exclusion contours at various confidence levels for $E_e = 60$ GeV – understandably, higher σ-contours demand larger luminosities. It is also seen that there is a kink around $\zeta_t = \pi/2$ such that for the region $0 < \zeta_t < \pi/2$, we need larger luminosities for exclusion. This is in keeping with the feature exhibited in Fig. 3 where the constructive interference between the signal diagrams enhances the cross-section over the SM value much more for $\zeta_t > \pi/2$ thus requiring less luminosity to probe that region. For $L = 100$ fb^{-1}, regions above $\pi/5 < \zeta_t \leq \pi$ and $3\pi/10 < \zeta_t \leq \pi$ are excluded at 2σ and 3σ C.L. While around $L = 400$ fb^{-1}, regions above $\pi/6 < \zeta_t \leq \pi$ and $\pi/4 < \zeta_t \leq \pi$ are excluded at 4σ and 5σ C.L. respectively.

For higher $E_e = 120$ GeV, the cross section for signal (background) is enhanced approximately by a factor of 4 (3) and hence the luminosity required for exclusion is smaller compared to the

---

[3] Polar angle $\cos\theta_{ij}(p_i, p_j)$ between two final state particles i and j with four-momentum p_i and p_j respectively is defined as the angle between direction of p_i in the rest frame of $p_i + p_j$ and the direction of $p_i + p_j$ in the lab frame.
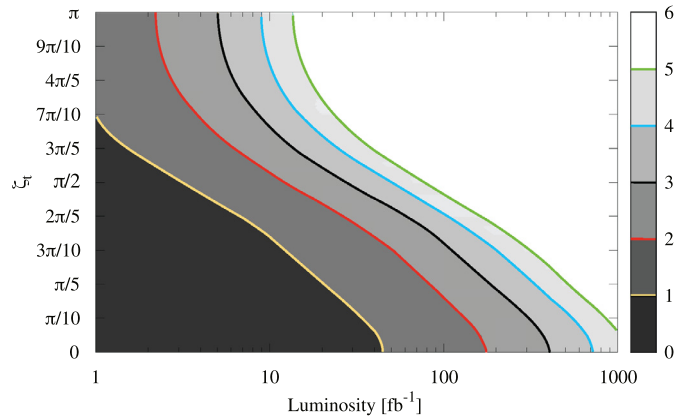
Fig. 8. The exclusion contour with respect to integrated luminosities at various ζ_t by considering significance based on fiducial cross section (defined in text) for $E_e = 60$ GeV and $E_p = 7$ TeV. The regions beyond each contour are excluded for the particular luminosity, *black* and *red* solid lines correspond to 3σ and 2σ regions. (For interpretation of the references to colour in this figure legend, the reader is referred to the web version of this article.)

$E_e = 60$ GeV case. Specifically, at $L = 100$ fb^{-1} regions above $\pi/20 < \zeta_t \leq \pi$ and $\pi/6 < \zeta_t \leq \pi$ are excluded at 4σ and 5σ C.L. We note, as a measure of comparison, that asymmetry studies at the HL-LHC [17] help probe up to $\zeta_t = \pi/6$ for a total integrated luminosity of 3 ab^{-1}. Thus, it is clear that the LHeC provides a better environment to test the CP nature of Higgs boson couplings.

Hence it is apparent that the method based on fiducial inclusive cross sections results in better limits than the asymmetry observable. It is interesting to note that for the design luminosity $L = 1$ ab^{-1}, almost all values of ζ_t are excluded up to 4σ C.L. While investigating the overall sensitivity of ζ_t by applying these two observables, it is also important to measure the accuracy of SM tth coupling κ at the LHeC energies. To measure the accuracy of κ by using signal and background yields we use the formula $\mathcal{K} = \sqrt{(S+B)}/(2S)$ at a particular luminosity. And for $E_e = 60$ (120) GeV, the measured accuracy at the design luminosity $L = 1$ ab^{-1} is given to be $\kappa = 1.00 \pm 0.17$ (0.08) of its expected SM value, where a 10% systematic uncertainty is taken in background yields only.

4. Summary and conclusions

The discovery of a Higgs with properties very close to that predicted in the SM has necessitated experiments that help us elucidate the nature of its couplings. While any deviation in Higgs boson couplings to WW and ZZ would unambiguously provide clues for a modified electroweak symmetry breaking sector, any possible pseudoscalar admixture in the physical Higgs boson is more easily manifest in its couplings to fermions. One promising avenue is the elucidation of such modifications in the tth coupling – owing to the large Yukawa, this is the most obvious channel. While the LHC is a top factory, coupling determination in pp colliders is usually fraught with difficulty. The e^+e^- machine provides a cleaner environment but one generally has to contend with smaller cross-sections. A third possibility is an e^-p machine – while this does not compete with the LHC in terms of absolute cross-sections, the intrinsic asymmetric nature of the machine (because of the difference in the e^- and p energies) provides certain advantages. In this letter, we analysed the question of uncovering possible CP-odd components in the tth coupling at the LHeC.

Using the associated top-Higgs production and based on different observables as a function of CP-phase ζ_t of tth-coupling, we observe different distinguishable features. The difference between

rapidities of anti-top quark and Higgs-boson Δy_{ht}, and anti-top polarisation P_t show unique features that are distinct from the pure scalar type couplings.

Considering the leptonic decay mode of the anti-top quark and $h \rightarrow b\bar{b}$, we constructed the asymmetry observables $\Delta\phi_{b_1 l^-}$ and $\cos\theta_{b_1 l^-}$. We find that while these show deviations from the SM case in the region $0 < \zeta_t \leq \pi/2$, the curves flatten out beyond that point. This prompted us to construct yet another observable $\cos\theta_{b_2 l^-}$ whose variation with ζ_t is significant in the entire range $0 < \zeta_t \leq \pi$.

Somewhat counterintuitively, exclusion regions for ζ_t obtained through fiducial cross section considerations result in better limits than those using asymmetry measurements. Quite strikingly, we find that almost all values of ζ_t can be excluded at 2σ (4σ) with an integrated luminosity of 200 fb^{-1} (700 fb^{-1}) – these limits are superior to those found in studies at the HL-LHC. While the limits would possibly worsen when one does a full detector level simulation, our analysis gives excellent early signs for the efficacy of the LHeC for coupling measurements.

We conclude that a study of cross-section measurements combined with accurate measurements of kinematic observables can be a powerful probe at the LHeC to uncover the finer details of the nature of the top-Higgs coupling and hope that this study adds to the physics goals of future e^-p colliders.

As mentioned in Section 2, apart from tth coupling the process considered in this study involves hWW and Wtb couplings as well where non-standard anomalous contributions are not negligible – these are studied in Refs. [11,18] and [19] respectively. Since the gauge–scalar (WWh) and gauge–fermion (Wtb) anomalous couplings involve momentum dependent couplings, the differential distribution of final state particles is affected differently via such effects and can thus be used as an effective discriminant to disentangle the effects of different new physics contributions to the process under investigation. For future studies, a global analysis involving all anomalous non-standard couplings together will be helpful to investigate the potential of precision measurement capabilities of collider facilities like the LHeC.

Acknowledgements

References

[1] G. Aad, et al., Observation of a new particle in the search for the standard model Higgs boson with the ATLAS detector at the LHC, Phys. Lett. B 716 (2012) 1–29, http://dx.doi.org/10.1016/j.physletb.2012.08.020, arXiv:1207.7214.

[2] S. Chatrchyan, et al., Observation of a new boson at a mass of 125 GeV with the CMS experiment at the LHC, Phys. Lett. B 716 (2012) 30–61, http://dx.doi.org/10.1016/j.physletb.2012.08.021, arXiv:1207.7235.

[3] G. Aad, et al., Measurement of the Higgs boson mass from the $H \rightarrow \gamma\gamma$ and $H \rightarrow ZZ^* \rightarrow 4\ell$ channels with the ATLAS detector using 25 fb^{-1} of pp collision data, Phys. Rev. D 90 (5) (2014) 052004, http://dx.doi.org/10.1103/PhysRevD.90.052004, arXiv:1406.3827.

[4] V. Khachatryan, et al., Precise determination of the mass of the Higgs boson and tests of compatibility of its couplings with the standard model predictions using proton collisions at 7 and 8 TeV, Eur. Phys. J. C 75 (5) (2015) 212, http://dx.doi.org/10.1140/epjc/s10052-015-3351-7, arXiv:1412.8662.

[5] G. Aad, et al., Combined measurement of the Higgs boson mass in pp collisions at $\sqrt{s} = 7$ and 8 TeV with the ATLAS and CMS experiments, Phys. Rev. Lett. 114 (2015) 191803, http://dx.doi.org/10.1103/PhysRevLett.114.191803, arXiv: 1503.07589.

[6] G. Aad, et al., Study of the spin and parity of the Higgs boson in diboson decays with the ATLAS detector, Eur. Phys. J. C 75 (10) (2015) 476, http://dx.doi.org/10.1140/epjc/s10052-016-3934-y, arXiv:1506.05669;
G. Aad, et al., Eur. Phys. J. C 76 (3) (2016) 152 (Erratum).

[7] V. Khachatryan, et al., Constraints on the spin-parity and anomalous HVV couplings of the Higgs boson in proton collisions at 7 and 8 TeV, Phys. Rev. D 92 (1) (2015) 012004, http://dx.doi.org/10.1103/PhysRevD.92.012004, arXiv: 1411.3441.

[8] J.L. Abelleira Fernandez, et al., A Large Hadron electron Collider at CERN: report on the physics and design concepts for machine and detector, J. Phys. G 39 (2012) 075001, http://dx.doi.org/10.1088/0954-3899/39/7/075001, arXiv: 1206.2913.

[9] O. Bruening, M. Klein, The Large Hadron electron Collider, Mod. Phys. Lett. A 28 (16) (2013) 1330011, http://dx.doi.org/10.1142/S0217732313300115, arXiv: 1305.2090.

[10] T. Han, B. Mellado, Higgs boson searches and the $Hb\bar{b}$ coupling at the LHeC, Phys. Rev. D 82 (2010) 016009, http://dx.doi.org/10.1103/PhysRevD.82.016009, arXiv:0909.2460.

[11] S.S. Biswal, R.M. Godbole, B. Mellado, S. Raychaudhuri, Azimuthal angle probe of anomalous HWW couplings at a high energy ep collider, Phys. Rev. Lett. 109 (2012) 261801, http://dx.doi.org/10.1103/PhysRevLett.109.261801, arXiv: 1203.6285.

[12] A. Kobakhidze, N. Liu, L. Wu, J. Yue, Implications of CP-violating top-Higgs couplings at LHC and Higgs factories, Phys. Rev. D 95 (1) (2017) 015016, http://dx.doi.org/10.1103/PhysRevD.95.015016, arXiv:1610.06676.

[13] V. Cirigliano, W. Dekens, J. de Vries, E. Mereghetti, Is there room for CP violation in the top-Higgs sector?, Phys. Rev. D 94 (1) (2016) 016002, http://dx.doi.org/10.1103/PhysRevD.94.016002, arXiv:1603.03049.

[14] V. Cirigliano, W. Dekens, J. de Vries, E. Mereghetti, Constraining the top-Higgs sector of the standard model effective field theory, Phys. Rev. D 94 (3) (2016) 034031, http://dx.doi.org/10.1103/PhysRevD.94.034031, arXiv:1605.04311.

[15] A. Kobakhidze, L. Wu, J. Yue, Anomalous top-Higgs couplings and top polarisation in single top and Higgs associated production at the LHC, J. High Energy Phys. 10 (2014) 100, http://dx.doi.org/10.1007/JHEP10(2014)100, arXiv: 1406.1961.

[16] J. Li, Z.-g. Si, L. Wu, J. Yue, Central-edge asymmetry as a probe of Higgs-top coupling in $t\bar{t}h$ production at LHC, arXiv:1701.00224.

[17] S.D. Rindani, P. Sharma, A. Shivaji, Unraveling the CP phase of top-Higgs coupling in associated production at the LHC, Phys. Lett. B 761 (2016) 25–30, http://dx.doi.org/10.1016/j.physletb.2016.08.002, arXiv:1605.03806.

[18] M. Kumar, X. Ruan, R. Islam, A.S. Cornell, M. Klein, U. Klein, B. Mellado, Probing anomalous couplings using di-Higgs production in electron–proton colli-

sions, Phys. Lett. B 764 (2017) 247–253, http://dx.doi.org/10.1016/j.physletb.2016.11.039, arXiv:1509.04016.

[19] S. Dutta, A. Goyal, M. Kumar, B. Mellado, Measuring anomalous Wtb couplings at $e^- p$ collider, Eur. Phys. J. C 75 (12) (2015) 577, http://dx.doi.org/10.1140/epjc/s10052-015-3776-z, arXiv:1307.1688.

[20] A. Alloul, N.D. Christensen, C. Degrande, C. Duhr, B. Fuks, FeynRules 2.0 – a complete toolbox for tree-level phenomenology, Comput. Phys. Commun. 185 (2014) 2250–2300, http://dx.doi.org/10.1016/j.cpc.2014.04.012, arXiv: 1310.1921.

[21] J. Alwall, R. Frederix, S. Frixione, V. Hirschi, F. Maltoni, O. Mattelaer, H.S. Shao, T. Stelzer, P. Torrielli, M. Zaro, The automated computation of tree-level and next-to-leading order differential cross sections, and their matching to parton shower simulations, J. High Energy Phys. 07 (2014) 079, http://dx.doi.org/10.1007/JHEP07(2014)079, arXiv:1405.0301.

[22] R.D. Ball, et al., Parton distributions with LHC data, Nucl. Phys. B 867 (2013) 244–289, http://dx.doi.org/10.1016/j.nuclphysb.2012.10.003, arXiv:1207.1303.

[23] C.S. Deans, Progress in the NNPDF global analysis, in: Proceedings, 48th Rencontres de Moriond on QCD and High Energy Interactions, La Thuile, Italy, March 9–16, 2013, 2013, pp. 353–356, arXiv:1304.2781, https://inspirehep.net/record/1227810/files/arXiv:1304.2781.pdf.

[24] G. Aad, et al., Measurements of the Higgs boson production and decay rates and constraints on its couplings from a combined ATLAS and CMS analysis of the LHC pp collision data at $\sqrt{s} = 7$ and 8 TeV, J. High Energy Phys. 08 (2016) 045, http://dx.doi.org/10.1007/JHEP08(2016)045, arXiv:1606.02266.

[25] S. von Buddenbrock, N. Chakrabarty, A.S. Cornell, D. Kar, M. Kumar, T. Mandal, B. Mellado, B. Mukhopadhyaya, R.G. Reed, The compatibility of LHC Run 1 data with a heavy scalar of mass around 270 GeV, arXiv:1506.00612.

[26] S. von Buddenbrock, N. Chakrabarty, A.S. Cornell, D. Kar, M. Kumar, T. Mandal, B. Mellado, B. Mukhopadhyaya, R.G. Reed, X. Ruan, Phenomenological signatures of additional scalar bosons at the LHC, Eur. Phys. J. C 76 (10) (2016) 580, http://dx.doi.org/10.1140/epjc/s10052-016-4435-8, arXiv:1606.01674.

[27] A. Kruse, A.S. Cornell, M. Kumar, B. Mellado, X. Ruan, Probing the Higgs boson via vector boson fusion with single jet tagging at the LHC, Phys. Rev. D 91 (5) (2015) 053009, http://dx.doi.org/10.1103/PhysRevD.91.053009, arXiv: 1412.4710.

[28] M. Aaboud, et al., Measurement of the top quark mass in the $t\bar{t} \rightarrow$ dilepton channel from $\sqrt{s} = 8$ TeV ATLAS data, Phys. Lett. B 761 (2016) 350–371, http://dx.doi.org/10.1016/j.physletb.2016.08.042, arXiv:1606.02179.

[29] W. Bernreuther, Top quark physics at the LHC, J. Phys. G 35 (2008) 083001, http://dx.doi.org/10.1088/0954-3899/35/8/083001, arXiv:0805.1333.

[30] A. Czarnecki, M. Jezabek, J.H. Kuhn, Lepton spectra from decays of polarized top quarks, Nucl. Phys. B 351 (1991) 70–80, http://dx.doi.org/10.1016/0550-3213(91)90082-9.

[31] A. Brandenburg, Z.G. Si, P. Uwer, QCD corrected spin analyzing power of jets in decays of polarized top quarks, Phys. Lett. B 539 (2002) 235–241, http://dx.doi.org/10.1016/S0370-2693(02)02098-1, arXiv:hep-ph/0205023.